minerals

MDPI

Article

RETRACTED: Insight into the Potential Antioxidant and Antidiabetic Activities of Scrolled Kaolinite Single Sheet (KNs) and Its Composite with ZnO Nanoparticles: Synergetic Studies

Hassan Ahmed Rudayni [1], Malak Aladwani [1], Lina M. Alneghery [1], Ahmed A. Allam [2], Mostafa R. Abukhadra [3,4,*] and Stefano Bellucci [5,*]

1 Department of Biology, College of Science, Imam Muhammad bin Saud Islamic University, Riyadh 11623, Saudi Arabia
2 Zoology Department, Faculty of Science, Beni-Suef University, Beni-Suef 65214, Egypt
3 Materials Technologies and Their Applications Lab, Geology Department, Faculty of Science, Beni-Suef University, Beni-Suef 65214, Egypt
4 Geology Department, Faculty of Science, Beni-Suef University, Beni-Suef 65214, Egypt
5 INFN, Laboratori Nazionali Di Frascati, E. Fermi 54, 00044 Frascati, Italy
* Correspondence: abukhadra89@science.bsu.edu.eg (M.R.A.); bellucci@lnf.infn.it (S.B.)

Abstract: The kaolinite sheets were scrolled by sonication-induced chemical delamination processes into well-developed nanotubes (KNs) which were used as substrates for microwave-based ZnO nanoparticles (ZnO/KNs). The biological activities of synthetic ZnO/KNs structures, in terms of the antioxidant and antidiabetic properties, were assessed in comparative studies with the separated phases of the synthetic ZnO and KNs as well as the commercially used ZnO. The KNs substrate resulted in a notable enhancement in the antioxidant and antidiabetic properties of ZnO, which was assigned positive influence on the surface area, interactive interfaces, charge separation, and agglomeration properties of ZnO in addition to the detectable bioactive properties of the KNs structure. The ZnO/KNs structure achieved remarkable scavenging efficiencies for 1, 1-diphenyl-2-picrylhydrazil (DPPH) (89.8 ± 1.57%), nitric oxide (90.6 ± 1.63%), 2,2′-azino-bis(3-ethylbenzothiazoline-6-sulphonic acid) (ABTS) (86.8 ± 1.28%), and superoxide (43.9 ± 1.72%) radicals. Additionally, it shows high inhibition effects on porcine α-amylase (84.3 ± 1.92%), crude α-amylase (70.6 ± 1.37%), pancreatic α-Glucosidase (94.7 ± 1.54%), crude α-Glucosidase (95.4 ± 1.64%), and amyloglucosidase (95.3 ± 1.32%) enzymes. This antidiabetic activity is significantly higher than the activity of miglitol and close to or slightly higher than acarbose, which leads us to recommend the use of ZnO/KNs when considering the cost and side effects of the commercially used drugs.

Keywords: kaolinite nano-scrolls; ZnO; microwave; antioxidant; antidiabetic

check for updates

Citation: Rudayni, H.A.; Aladwani, M.; Alneghery, L.M.; Allam, A.A.; Abukhadra, M.R.; Bellucci, S. RETRACTED: Insight into the Potential Antioxidant and Antidiabetic Activities of Scrolled Kaolinite Single Sheet (KNs) and Its Composite with ZnO Nanoparticles: Synergetic Studies. *Minerals* **2023**, *13*, 567. https://doi.org/10.3390/min13040567

Academic Editors: Michael Schmidt and Harold S. Bernhardt

Received: 20 February 2023
Revised: 13 April 2023
Accepted: 14 April 2023
Published: 18 April 2023
Retracted: 23 January 2026

Copyright: © 2023 by the authors. Licensee MDPI, Basel, Switzerland. This article is an open access article distributed under the terms and conditions of the Creative Commons Attribution (CC BY) license (https://creativecommons.org/licenses/by/4.0/).

1. Introduction

The eventual escalation in the number of confirmed diabetes patients in the contemporary world is one of the critical health issues facing health authorities, with the number of patients expected to increase to 366 million by 2030, thus becoming the seventh leading cause of death [1–3]. Diabetes is a known type of clinical pancreatic syndrome and is categorized into two common types: (1) type-1 (T1-DM) and (2) type-2 (T2-DM). Type-2, as a stark metabolic disorder, is the mostly detected diabetes type and might affect up to 90% of patients by 2030 [1,4]. Normally, it is associated with post-prandial hyperglycemia (abnormal glucose levels) and abnormal release of reactive free oxidizing radicals (reactive oxygen species (ROS)) [5,6]. Cardiomyopathy, polyphagia, kidney failure, coronary heart disease, polydipsia, morbidity, mortality, nephropathy, neuropathy, glycosuria, and retinopathy are the common types of clinical complications that are related to type-2 diabetes mellitus and abnormal levels of blood glucose [7–9]. Additionally, lipid peroxidation,

RETRACTED

insulin resistance, destruction of blood vessels, and damage of organelles were reported as pathophysiological side effects of the abnormal increase in the concentrations of ROS and their associated oxidative stresses [6,8,10,11].

Sulfonylureas, biguanides, a thiazolidinedione, voglibose, miglitol, and acarbose are widely used commercial drugs in the role as antidiabetic agents that cause significant declination in the levels of ROS radicals and hyperglycemia [6,8,12]. Unfortunately, several types of commonly used commercial drugs are expensive products, and their applications can cause notable health sides effects such as diarrhea, severe hypoglycemia, hepatotoxicity, meteorism, and abdomen distention [6,13]. Therefore, several materials of biologically active and multifunctional chemical groups were recommended as potential antidiabetic and antioxidant agents that can exhibit enhanced inhibition properties against essential enzymes and scavenging properties against ROS radicals [6,14]. Recently, metal oxides and their composites attracted wide attention as effective antioxidants and antidiabetic agents. Besides their low production cost and unique physicochemical properties, metal oxide nanoparticles are characterized by significant biological activity, therapeutic and theranostic potentiality, and biocompatibility [14–18]. Zinc oxide is one of the most investigated metal oxides as bioactive material that is characterized by its biocompatibility, nontoxicity, antidiabetic, and antioxidant properties [18–22]. The zinc element in the human body is one of the most biologically active and vital elements, and it is very effective during the formation reactions of nucleic acid and protein [15,20]. Therefore, zinc and zinc oxide are widely used in several biological, medical, and pharmaceutical applications including their use as drug carriers, antibacterial agents, anticancer agents, hypoglycemic agents, and antioxidant agents in addition to their vital role in the tissue engineering industry [15,23].

Recent research has widely documented the valuable antioxidant properties of ZnO nanoparticles, which can effectively regulate mitochondrial respiration, inhibit oxidant enzymes, and reduce oxidizing reactive oxygen free radicals [6,14]. The accumulation behaviors of the synthetic ZnO particles via van der Waals forces as well as their fast recombination rates and surficial properties cause significant declination in the generation efficiency of the free radicals and, in turn, their biological and photocatalytic properties [14,24]. Moreover, most of the presented results in the later periods declared the significant effects of the synthesis conditions, production methods, crystallite size, and morphological features on the biological and medical qualifications of synthetic ZnO particles [15,16,25]. Surface modifications and hybridization of the synthetic ZnO particles by the different physical and chemical methods were suggested as enhancement techniques for their biocompatibility, biological activity, and genotoxicity in addition to their antibacterial and antioxidant properties [15,18,26]. The commonly used modification techniques are: (1) elemental doping of ZnO crystal structure, (2) integrating the ZnO particles in composites with other metal oxides, (3) supporting the synthetic ZnO particles into effective carriers or substrates, (4) integrating the synthetic ZnO particles in composites with biologically active biopolymers, and (5) synthesis of the ZnO grains in chemical complexes with the known active phytochemicals from the extracts of the plants [14,20,27,28].

Materials that exhibit one-dimensional morphology, such as nanotubes and nanorods, were commended strongly either as catalyst supports or carriers for the bio-active structures [29]. This was assigned to the unique surface area of these structures and their significant dispersion properties [30,31]. Subsequently, the scrolled kaolinite that exhibits nanotube-like morphologies was investigated effectively as a potential carrier of catalysts or as a potential photocatalyst. The scrolled kaolinite is characterized by a high surface area, surface reactivity, dispersion properties, and highly ordered porous structures [29]. Therefore, its application as a carrier of the common photocatalysts strongly induces their activities, stability, free radical generation efficiencies, and recombination rates [29,32,33]. Moreover, several studies have been developed in recent times that demonstrated the significant photocatalytic properties of the clay nanostructures as a result of their metallic impurities [34]. Additionally, it was reported that the kaolinite structure exhibits electron-accepting and electron-donating sites [34,35]. Therefore, it was predicted that the kaolinite

RETRACTED

nanostructure in nano-scroll morphology will show considerable biological activity as an antioxidant and antidiabetic agent [34]. The presented study investigates for the first time the biological activities of synthetic kaolinite nano-scrolls (KNs) and their hybrid structure with ZnO nanoparticles formed under microwave irradiation as potential antioxidant and antidiabetic agents considering the synergetic effect of ZnO and KNs substrate. This involves the investigation of the scavenging efficiencies of the common oxidative radicals in addition to their inhibition effects on essential enzymes.

2. Experimental Work

2.1. Materials

The starting kaolinite was obtained from the Central Metallurgical Research and Development Institute, Egypt, and applied as raw materials during the formation of the kaolinite scrolls. The chemicals used during the synthesis procedures are: dimethyl sulfoxide (DMSO) (>99.5%; Sigma-Aldrich, Cairo, Egypt), cetyltrimethylammonium bromide (CTAB) (>98%; Sigma-Aldrich, Egypt), methanol (>99.9%; Sigma-Aldrich, Egypt), zinc nitrate hexahydrate (98%; Sigma-Aldrich, Egypt), and NaOH pellets (97%; Sigma-Aldrich, Egypt). α-amylase, 1,1-diphenyl-2-picrylhydrazil (DPPH), starch, α-glucosidase, 2′-azino-bis(3-ethylbenzothiazoline-6-sulphonic acid) (ABTS), para-nitrophenyl α-glucopyranoside (pNPG), 2, L-ascorbic acid, and phosphate buffer were applied during the biological antioxidant and antidiabetic tests (Sigma-Aldrich; Egypt).

2.2. Synthesis of the Composite

2.2.1. Scrolling of Kaolinite Sheets (KNs)

The kaolinite scrolls were obtained by common sonication-induced chemical expansion reactions. Firstly, this involved homogenization of the kaolinite powder (15 g) within about 50 mL of the diluted DMSO solution (80% DMSO: 10% water) as a strong organic reagent to destruct the strong hydrogen bonds between the kaolinite units. This step was conducted over 24 h under continuous stirring, and the obtained DMSO intercalated kaolinite product (DMSO/K) was washed extensively with distilled water followed by methanol washing runs. Five methanol washing runs were performed, and each run required about 20 min to obtain methoxy-modified kaolinite sheets (MX/K). The resulting MX/K particles were incorporated in chemical expansion processes involving homogenization of these fractions with CTAB solution (500 mL) for 48 h using a magnetic stirrer at an adjusted speed of 500 rpm. After that, the mixture was sonicated for an additional 48 h using an ultrasonic source of 240 W as a powder to ensure the scrolling of the separated kaolinite sheets into nanotubes. After this step, the product was extracted, washed extensively with distilled water, and dried to be incorporated in the next synthesis steps and future applications procedures.

2.2.2. Synthesis of ZnO Decorated KNs Structure (ZnO/KNs)

The synthesis procedures involved firstly homogenization of the synthetic KNs particles within previously prepared zinc nitrate aqueous solution (50 mL; 1M). The homogenization processes involved two cooperating mixing systems which consisted of a magnetic stirrer (500 rpm) and sonication source (240 W), and this step lasted about 60 min at room temperature. Then, an alkaline NaOH solution (0.5 M) was drop-wise incorporated into the synthesis system at a constant temperature (65 °C) until the first formation of a low-density white gel. The mixture after this observation was transferred into a tightly sealed Teflon autoclave and subjected to domestic microwave irradiation of 900 W power for 30 min. The synthetic solid product was separated and washed thoroughly for five cycles using distilled water to neutralize its surface from the rest of NaOH, dried gently for 10 h at 80 °C, and kept for further characterization and applications procedures. The synthesis procedures are presented schematically in Figure 1.

RETRACTED

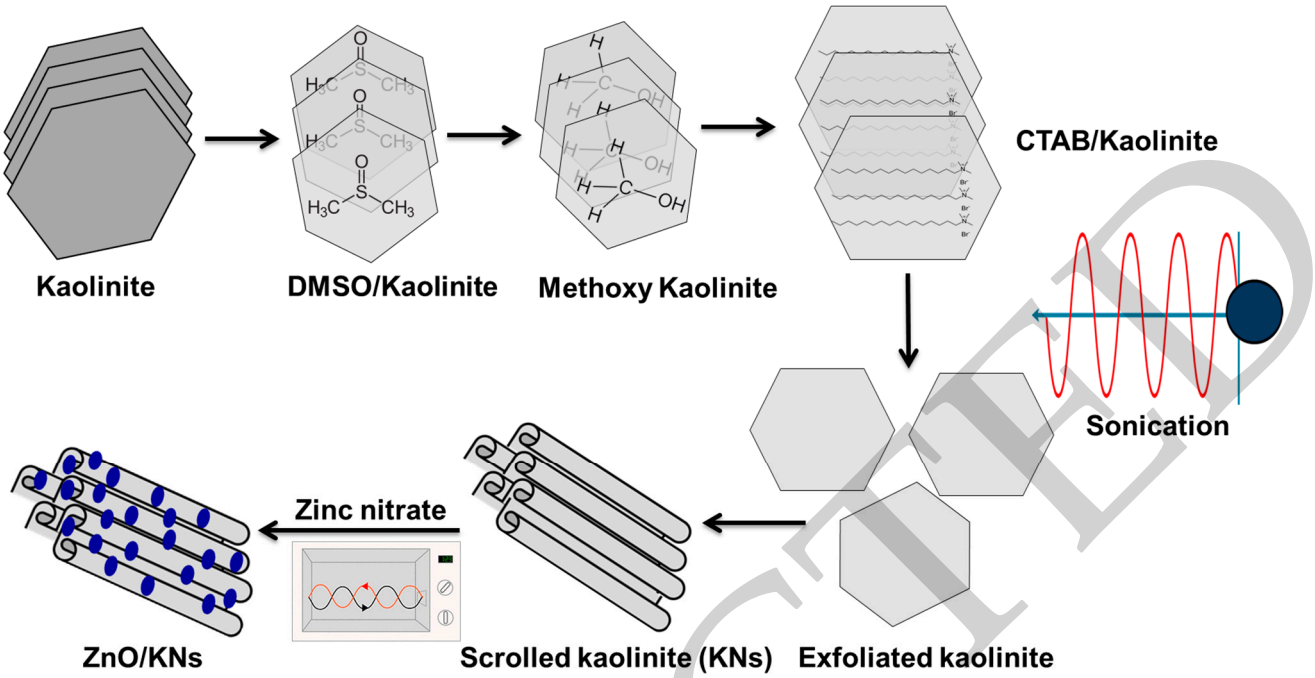


Figure 1. Schematic diagram for the synthesis procedures of KNs and ZnO/KNs composite.

2.3. Characterization Techniques

The structural properties and the obtained crystalline phases were identified and studied based on the determined X-ray diffraction patterns utilizing the PANalytical XRD diffractometer (Empyrean) with radiation source composed of Cu-Kα within measurement range from 5° to 80°. The elemental composition and the chemical functional groups were followed based on recognized EDX spectra by energy-dispersive X-ray (EDX) technique and FT-IR spectra by Fourier Transform Infrared spectrometer (FTIR−8400S) technique, respectively. The morphology as well as the internal properties of the synthetic structures (KNs and ZnO/KNs) was studied based on their SEM images by Scanning Electron-Microscope (Gemini-Zeiss, Ultra 55) and their HRTEM images by Transmission Electron Microscope (JEOL-JEM, 2100). Texturally, the surface area and pore size distribution were measured using a Beckman Coulter surface area analyzer (SA3100 type) depending on the plotted N_2 adsorption/desorption curves and after the analysis of the data according to Brunauer–Emmett–Teller (BET) and Barrett–Joyner–Halenda (BJH) techniques, respectively.

2.4. Antioxidant Studies

2.4.1. Scavenging of Nitric Oxide Radical

The scavenging properties of nitric oxide were assessed in a synergetic system considering the properties of commercial ZnO, microwave-synthesized ZnO, kaolinite nano-scrolls (KNs), and the synthetic ZnO/KNs composite. The scavenging tests were performed based on the signified steps by Kitture et al. [36]. The synthetic composite as well as the other evaluated materials were dispersed in addition to 2 mL of sodium nitroprusside (10 mM) within about 500 µL of phosphate buffer at pH 7.4. The obtained mixtures were incubated at 25 °C for 150 min and then homogenized with 1 mL of new reagent composed of diluted sulphanilic acid in which 33% of the sulphanilic acid was mixed with 20% of glacial acetic acid. This was followed by an additional incubation interval for 5 min, and then 1 mL of the naphthyl ethylenediamine dihydrochloride (0.1% *w*/*v*) reagent was incorporated in the incubated systems before their incubation again for 30 min. After attending the end of the incubation duration, the absorbance of the incubation systems in the existence of the

RETRACTED

materials and in the absence of them (controls) was detected using a microplate reader at 450 nm and applied to calculate the scavenging percentage, as in Equation (1).

$$\text{Scavenging } (\%) = \frac{\text{A540}_{\text{Control}} - \text{A540}_{\text{Test}}}{\text{A540}_{\text{Control}}} \times 100 \quad (1)$$

2.4.2. Scavenging of 1,1-Diphenyl-2-picrylhydrazil (DPPH) Radical

The reported scavenging procedures of DPPH by Robkhob et al. [6] were applied to estimate the efficiencies of the synthetic ZnO, KNs, and ZnO/KNs materials. Then, 20 µL of the investigated materials (100 µg/mL) was homogenized with about 80 µL of methanolic solutions in 96-well plates as individual tests, and the solutions were supplemented after that with 100 µM of 2, 2-diphenyl-1-picrylhydrazyl (DPPH). The obtained mixtures were incubated for 20 min in dark, and then the absorbance in the existence of the materials and in the absence of them (controls) was detected using a microplate reader at 517 nm and applied to calculate the scavenging percentage, as in Equation (2).

$$\text{Scavenging } (\%) = \frac{\text{A517}_{\text{Control}} - \text{A517}_{\text{Test}}}{\text{A517}_{\text{Control}}} \times 100 \quad (2)$$

2.4.3. Scavenging of 2,2-Azino-bis(3-ethylbenzothiazoline-6-sulphonic Acid) (ABTS) Radical

The reported scavenging procedures of ABTS by Dappula et al. [37] were applied to estimate the efficiencies of the synthetic ZnO, KNs, and ZnO/KNs materials. The ABTS solution was prepared by the complete dissolving of 44 mg of ABTS in deionized water (10 mL). The obtained aqueous solution was complemented with potassium persulfate (3 mm) as an essential reagent to produce the $ABTS^{\bullet+}$ free cations. The reaction systems were kept in the dark for 18 h at a constant temperature of 25 °C to confirm the effective generation of the $ABTS^{\bullet+}$ cations. After that, these systems were diluted carefully and gently with absolute methanol at a mixing ratio of 1:29 to obtain freshly made $ABTS^{\bullet+}$. Then, the synthetic materials (100 µg/mL) were homogenized within the ABTS solution (290 µL) for 30 min. After that, the absorbance of the incubation systems in the existence of the materials and in the absence of them (controls) was detected using a microplate reader at 734 nm and applied to calculate the scavenging percentage, as in Equation (3).

$$\text{Scavenging } (\%) = \frac{\text{A734}_{\text{Control}} - \text{A734}_{\text{Test}}}{\text{A734}_{\text{Control}}} \times 100 \quad (3)$$

2.4.4. Scavenging of Superoxide Radical

The reported scavenging procedures of superoxide ($O^{\bullet-}$) by Robkhob et al. [6] were applied to estimate the efficiencies of the synthetic ZnO, KNs, and ZnO/KNs materials. About 100 µL of the investigated and prepared materials was homogenized as individual tests within prepared mixtures consisting of EDTA (200 µL; 12 mM), NBT (100 µL; 0.1 mg), riboflavin (100 µL; 20 µg), and high-purity ethanol (200 µL). After that, the prepared mixtures were diluted with 3 mL of phosphate-buffered saline and kept under the effect of the light source for 5 min. After that, the absorbance of the incubation systems in the existence of the materials and in the absence of them (controls) was detected using a microplate reader at 540 nm and applied to calculate the scavenging percentage, as in Equation (1).

2.5. Antidiabetic Studies

2.5.1. Inhibition Assay of Porcine Pancreatic α-Amylase

The inhibition effects of ZnO, KNs, and ZnO/KNs on the commercially tested pancreatic α-amylase enzyme were investigated following the reported procedures by Robkhob et al. [6]. The synthetic ZnO, KNs, and ZnO/KNs materials were homogenized at certain dosages (100 µg/mL) with the evaluated commercial α-amylase enzyme (50 µg/mL). The obtained systems were incubated separately at a constant temperature of 37 °C for 10 min

RETRACTED

before the supplementation of the systems with starch (1%) as the incorporated substrate. After that, the absorbance of the incubation systems in the existence of the materials and in the absence of them (controls) was detected using a microplate reader at 540 nm and applied to calculate the inhibition percentage, as in Equation (4).

$$\text{Inhibition } (\%) = \frac{\text{A540}_{\text{Control}} - \text{A540}_{\text{Test}}}{\text{A540}_{\text{Control}}} \times 100 \quad (4)$$

2.5.2. Inhibition Assay of Crude Murine Pancreatic α-Amylase

This assay was performed to assess the inhibition effects of ZnO, KNs, and ZnO/KNs on the crude enzyme as well as the commonly tested commercial type of the α-amylase enzyme. The crude enzyme was extracted from the pancreas of a Swiss male mouse (10 weeks old) after its starvation for 12 h. This was followed by excision and immersion of the pancreas within phosphate-buffered solution, which was supplemented with protease inhibitors. The obtained cell-free supernatant was extracted by centrifugation step for 15 min at an adjusted speed of 10,000 rpm. Then, the system was diluted regularly until the determination of 0.4 as absorbance at a measuring wavelength of 280 nm. At this condition, the treated pancreas can be used effectively as a source of crude α-amylase enzyme. The inhibition assay of the assessed crude enzyme was completed according to the reported procedures in Section 2.5.2.

2.5.3. Inhibition Assay of α-Glucosidase

The inhibition effects of ZnO, KNs, and ZnO/KNs on the commercially tested α-Glucosidase enzyme were investigated following the reported procedures by Sanap et al. [38]. The synthetic ZnO, KNs, and ZnO/KNs materials were homogenized at certain dosages (100 µg/mL) with the evaluated commercial α-glucosidase enzyme (100 µL; 0.1 unit/mL). The obtained systems of ZnO, KNs, and ZnO/KNs were incubated separately at a constant temperature of 37 °C for 60 min before the supplementation of these systems with pNPG (10 mL) and their re-incubation again for 10 min. Finally, the reactions in the systems were stopped using 2 mL of Na_2CO_3 aqueous solution (0.1 M). After that, the absorbance of the released nitrophenol from pNPG in the systems in the existence of the materials and in the absence of them (controls) was detected using a microplate reader at 420 nm and applied to calculate the inhibition percentage, as in Equation (5).

$$\text{Inhibition } (\%) = \frac{\text{A420}_{\text{Control}} - \text{A420}_{\text{Test}}}{\text{A420}_{\text{Control}}} \times 100 \quad (5)$$

2.5.4. Inhibition Assay of Crude Murine Intestinal α-Glucosidase

The crude intestinal α-glucosidase was obtained according to the same reported procedures in Section 2.5.2. The inhibition assay experiments using ZnO, KNs, and ZnO/KNs against the intestinal α-glucosidase enzyme were conducted based on the previously reported steps during the evaluation of the commercial enzyme, as in Section 2.5.3, considering the incorporation of p-nitrophenyl-α-D-glucopyranoside as a substrate.

2.5.5. Amyloglucosidase Inhibition Assay

The inhibition effects of ZnO, KNs, and ZnO/KNs on the commercially tested amyloglucosidase enzyme were investigated following the reported procedures by Lawande et al. [39]. The synthetic ZnO, KNs, and ZnO/KNs materials were homogenized at certain dosages (100 µg/mL) with the evaluated amyloglucosidase enzyme (0.1 unit/mL). The obtained systems of ZnO, KNs, and ZnO/KNs were incubated separately at a constant temperature of 37 °C for 10 min in the presence of 1% starch as the incorporated substrate. After that, the absorbance of the incubation systems in the existence of the materials and in the absence of them (controls) was detected using a microplate reader at 540 nm and applied to calculate the inhibition percentage as in Equation (4).

RETRACTED

2.6. Statistical Analysis

The obtained results were presented and plotted as mean values ± the obtained standard errors of the detected mean values (S.E.M.) considering *n* a value less than 3. The accuracy and significance of the statistical assessment procedures were evaluated according to the analysis of the variance (ANOVA) in addition to the paired tests considering * *p* values < 0.05.

3. Results and Discussion

3.1. Characterization of the Synthetic Structures

The synthesis of the KNs and its composite with ZnO from raw kaolinite was followed based on the XRD patterns (Figure 2). The estimated patterns of the used precursor demonstrate the existence of the kaolinite identification peaks at 12.33° (001), 20.85° (−110), 24.87° (002), and 26.64° (111) with its characteristic basal spacing value 0.72 nm (Figure 2A). After the intercalation step with the DMSO molecules (DMSO/K), the resulting pattern demonstrated a significant reduction in the main detectable peaks of raw kaolinite (Figure 2B). The relicts peaks corresponding to the (001) and (002) crystallographic planes were observed as relatively broad and deviated peaks (Figure 2B). This signifies the structural effect of the DMSO intercalation reactions and the expected destruction of the hydrogen bonds, which is associated with enlargement in the basal spacing to 1.12 nm. The same structural observations were also recognized from the pattern of the methoxy-modified sample (MX/K) but with a greater reduction in the intensities of the peaks, deviation in the positions of the remaining peaks, and declination in the basal spacing value (0.92 nm) as compared to the DMSO/K particles (Figure 2C). The successful scrolling of the kaolinite into nano-scrolls or nanotubes was confirmed by the complete reduction in all the kaolinite peaks and the detection of a new reduced peak at 10.63° (001) (Figure 2D). The formation of a ZnO/KNs hybrid structure also was signified based on the identified diffraction peaks. The obtained pattern significantly demonstrates the existence of the ZnO (wurtzite) identification peaks (31.7° (100), 34.4° (002), and 36.2° (101)) (Figure 2E) (JCPDS no. 65-3411; JCPDS no. 36-1451), in addition to the marked peak of KNs, but at a slightly deviated position and reduced intensity as a result of the precipitation of ZnO on its surface (Figure 2E).

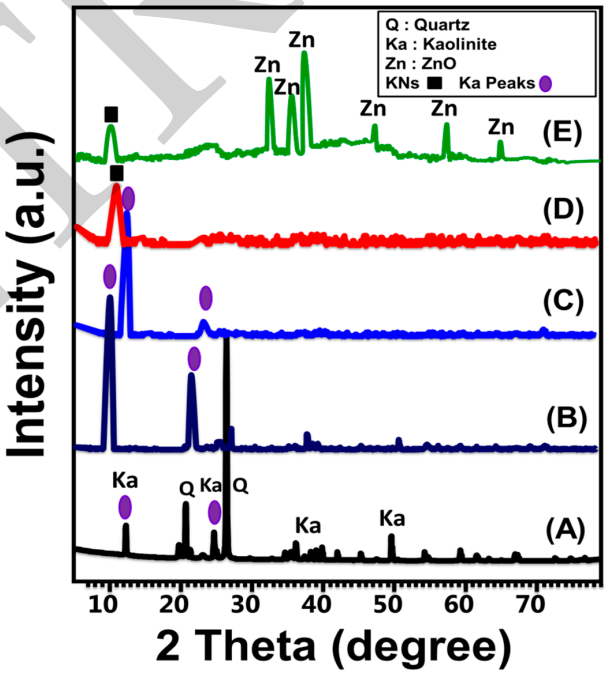


Figure 2. The XRD patterns of raw kaolinite (**A**), DMSO-intercalated kaolinite (**B**), methoxy kaolinite (**C**), synthetic scrolled kaolinite (KNs) (**D**), and synthetic ZnO/KN composite (**E**).

RETRACTED

The structural findings which were obtained based on the XRD analysis were confirmed by the other chemical analyses. The FT-IR spectrum of kaolinite demonstrated its widely identified chemical groups such as Si-OH (3689 cm^{-1}), Al-OH (912 and 3500 cm^{-1}), OH bending (1641 cm^{-1}), Si-O (456–787 cm^{-1}), Si-O-Al (526–680 cm^{-1}), and Si-O-Si (1020 cm^{-1}) (Figure 3A) [40,41]. The obtained spectrum of KNs show the previously reported chemical groups of kaolinite, but the assigned bands exhibit slight deviation in their positions. This was attributed to the expected destruction of the original hydrogen bonds and the formation of new bonds during the intercalation processes (Figure 3B) [42]. Regarding the spectrum of ZnO/KNs in comparison with the pure KNs, the existence of the same functional groups of the aluminosilicate structure of KNs is demonstrated, but with considerable deviation in the corresponding bands. Moreover, two new bands were observed around 466.3 cm^{-1} and 524 cm^{-1}, which signifies the stretching of O-Zn-O (Figure 3C) [24,43].

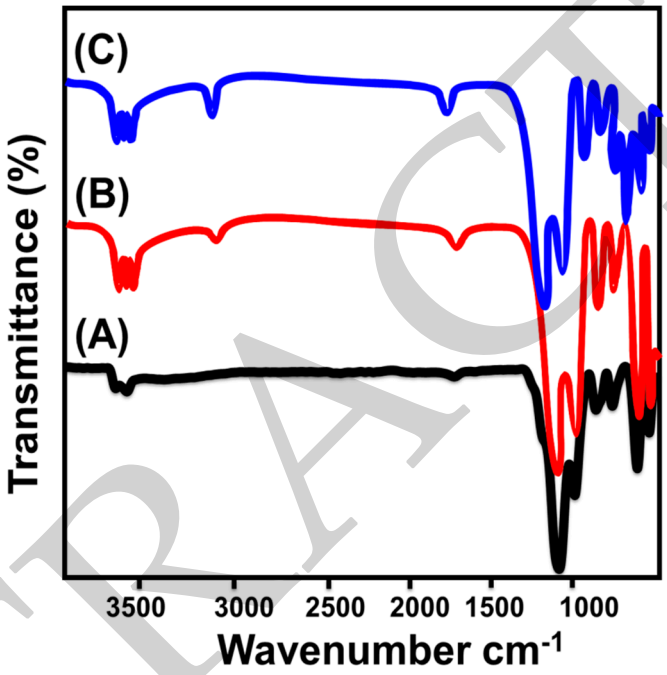


Figure 3. FT–IR spectra of raw kaolinite (**A**), synthetic scrolled kaolinite (KNs) (**B**), and synthetic ZnO/KNs composite (**C**).

This also confirms the formation of the composite and is in remarkable agreement with the EDX analysis (Figure 4). The elemental composition of the synthetic ZnO/KNs structure according to the EDX spectrum reflects the existence of Si, Al, and O elements which signify the structural silica tetrahedron and alumina octahedron of the kaolinite phyllosilicate structure in addition to the high abundance of the Zn element, which signifies the integrated ZnO nanoparticles (Figure 4). Moreover, the EDS mapping of the structure reflects the homogenous distribution of the supported ZnO nanoparticles throughout the surface of KNs as substrate (Figure S1 in the Supplementary Materials).

The SEM and HRTEM images were used to detect the morphological features and follow the successful integration between ZnO and KNs particles (Figure 5). The starting kaolinite powder either in the SEM or HRTEM images validates the characteristic features of the well-crystalline kaolinite grains as pseudo-hexagonal flakes of well-developed outlines (Figure 5A,B). The obtained images of the synthetic KNs demonstrate the effective conversion of the kaolinite flakes into observable nano-scrolls with remarkable tabular morphology in the SEM images (Figure 5C). This reveals the successful delamination of the incorporated kaolinite structure and the strong bending or folding of its units into tabular grains. The inspected HRTEM images of KNs significantly demonstrated the scrolling

RETRACTED

and bending of kaolinite flakes into highly ordered nanotubes with clear internal hollow structures (Figure 5D). Based on both the SEM and HRTEM images of KNs, the synthetic tubes or scrolls were formed within a length range from 50 nm up to 600 nm and exhibit an outer diameter within the range from 10 nm up to 20 nm, while the estimated range of the internal diameter was detected from 2 nm up to 20 nm (Figure 5D). Regarding the SEM images of ZnO/KNs particles, the supported ZnO particles were detected clearly as spherical or granular grains on the surface of the KNs substrates (Figure 5E). This was detected notably in the HRTEM images, as the KNs tabular particles appeared to be nearly coated with numerous ZnO nanoparticles (Figure 5F).

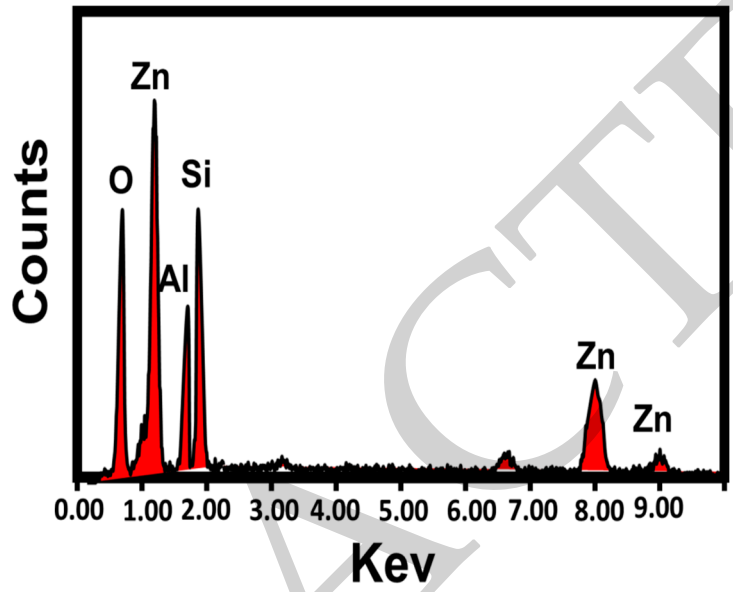


Figure 4. EDX spectrum of the synthetic ZnO/KNs composite.

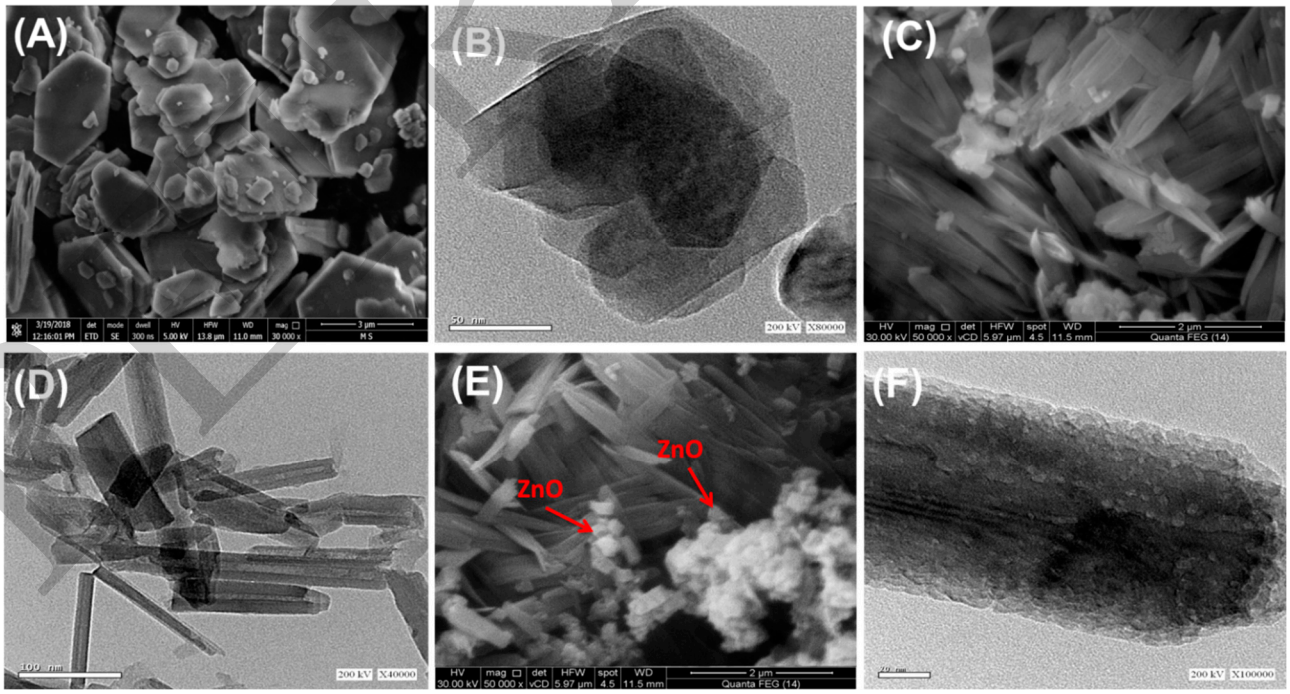


Figure 5. SEM image of raw kaolinite (**A**), HRTEM image of kaolinite (**B**), SEM image of synthetic KNs (**C**), HRTEM image of synthetic KNs (**D**), SEM image of synthetic ZnO/KNs (**E**), and HRTEM image of synthetic ZnO/KNs (**F**).

REJECTED

Texturally, both KNs and ZnO/KNs show IV-type N_2 adsorption/desorption isotherm curves with a noticeable H3 hysteresis loop (Figure S2 in the Supplementary Materials). This signifies the nonporous materials that exhibit cylindrical-like or tabular internal pores that might be formed by capillary condensation mechanisms [44]. The marked declination in the quantities of the adsorbed/desorbed nitrogen by ZnO/KNs as compared to KNs validates the adverse impact of supported ZnO on the porosity of KNs particles. The determined surface area, pore volume, and average pore diameter of KNs are 105 m^2/g, 0.51 cm^3/g, and 12 nm, respectively, while the measured values or ZnO/KNs are 95.4 m^2/g (surface area), 0.13 cm^3/g (pore volume), and 5.8 nm (average pore diameter).

3.2. Antioxidant Properties

3.2.1. Nitric Oxide Scavenging

The free reactive oxygen radicals normally generated during the aerobic respiration reactions, in addition to the electron transportation processes and their generation at abnormal levels, resulted in significant oxidative stresses as well as several species of degenerative diseases [45]. Nitric oxide (NO) was classified as an essential gaseous-free species of these reactive radicals, and its abnormal generation is associated with hazardous health drawbacks [6,46]. Fragmentation of DNA, cell cytotoxicity, death of the neuronal cells, and damage of cells are the commonly reported health side effects of the existence of abnormal concentrations of NO radicals [47]. The common species of bioactive metal oxides and their composites were assigned as potential materials that can exhibit promising scavenging for the generated NO radicals. The scavenging properties of ZnO/KNs were assessed in synergetic design considering the properties of KNs, microwave-induced synthesis of ZnO (M.ZnO), and commercial ZnO (C.ZnO), and in the existence of ascorbic acid as control or standard (Figure 6A). The determined scavenging % of NO radical by commercial ZnO, microwave-assessed ZnO, and KNs particles is 35.7 $\pm$ 1.57%, 36.4 $\pm$ 1.54%, and 18.6 $\pm$ 1.11%, respectively (Figure 6A). These results demonstrate considerable antioxidant properties of the synthetic scrolled kaolinite single sheets. The previously reported efficiencies enhanced notably after the combination between ZnO and KNs in composites (ZnO/KNs) achieving scavenging percentage of 90.6 $\pm$ 1.23%, which is also significantly higher than the determined efficiency using the ascorbic acid control (21.6 $\pm$ 1.33%) (Figure 6A).

The previously marked enhancement in the scavenging properties of ZnO/KNs as compared to the individual components is in agreement with previous research on the impact of the substrate on the bioactive properties of ZnO [26,46]. The KNs substrate significantly induces the surface area of ZnO, reduces the agglomeration affinities of the formed ZnO, and enhances the exposure interface of ZnO as the bioactive component [24,29,48]. The enhancement in the surface reactivity of scrolled kaolinite sheets and the high exposure of the active hydroxyl groups provides active interaction centers with the oxidizing radicals and in turn induces scavenging properties of the composite [34,49]. Moreover, the reported photocatalytic activity of clay nano-sheets as a result of its metallic content and the reported electron-accepting/electron-donating properties of kaolinite can prompt the generation quantities of the surficial electrons [48,50]. It was reported that the electron-supplying capacity of the assessed materials as antioxidant agents is the controlling factor during the experimental assessment of their qualifications as they pair significantly with the lone pairs of the hydroxyl radicals [48,50,51]. Therefore, the integration between ZnO and KNs in a hybrid structure can result in a promising multifunctional antioxidant product of enhanced efficiency.

RETRACTED

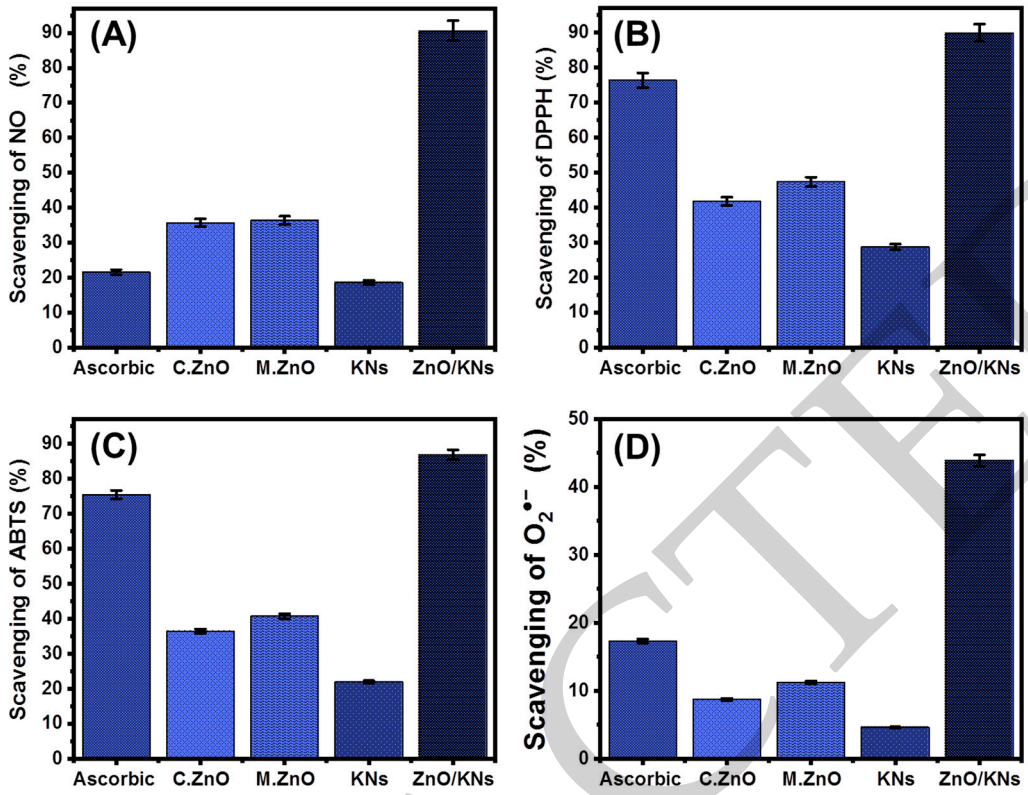


Figure 6. The antioxidant activities of C.ZnO, M.ZnO, KNs, and ZnO/KNs structures in the presence of ascorbic acid as positive control (the tests were replicated 5 times); (**A**) Nitric oxide scavenging activities; (**B**) DPPH scavenging activities with significantly higher activity for ZnO/KNs than ascorbic acid; (**C**) ABTS scavenging activities; and (**D**) super oxide radical scavenging activities with significantly higher activity for ZnO/KNs than ascorbic acid.

3.2.2. DPPH Radical Scavenging

The properties of M.ZnO, KNs, and ZnO/KNs as tested scavengers of DPPH were studied in comparison with commercial ZnO nanoparticles as well as the ascorbic acid control. The determined DPPH scavenging % by the tested structure exhibits the same behaviors as detected during the trapping of NO (Figure 6B). The recognized scavenging properties of ZnO/KNs (89.8 ± 1.57%) reflect its higher activity as compared to C.ZnO (41.7 ± 1.58%), M.ZnO (47.3 ± 1.86%), and KNs particles (28.7 ± 1.71%) (Figure 6B). This reflects enhancement by more than 42% as compared to M.ZnO, 62% as compared to KNs particles, and by about 13% as compared to the tested ascorbic acid standard (76.3 ± 1.28%) (Figure 6B). The scavenging mechanisms of the DPPH radical on the metal oxides-based antioxidants were caused by types of pair electron (e^-)/proton (H^+) transfer reactions from the surfaces of these structures to the organic structures of the target DPPH radical [37,52]. The supporting of ZnO into the scrolled kaolinite nanostructure with its significant hydroxyl group, considerable photocatalytic activity, and electron-accepting/electron-donating properties can induce notably the production efficiency of the electrons on the surface of the composite (ZnO/KNs) as well as the charge separation properties which effectively induce its antioxidant potentiality [53,54].

3.2.3. ABTS Radical Scavenging

The properties of M.ZnO, KNs, and ZnO/KNs as potential scavengers of ABTS were later evaluated as recommended techniques which can give significant indications about the antioxidant properties of the synthetic materials, especially synthetic composites or hybrid materials. This can be recognized by following the declination in the concentration of the generated ABTS cations ($ABTS^{\bullet+}$) in the system considering the existence of potassium

RETRACTED

persulfate as the used generation reagent. The synthetic or tested materials that exhibit remarkable hydrogen-donating antioxidant behaviors can be applied effectively during the scavenging of the $ABTS^{\bullet+}$ radical. Therefore, the commonly tested biologically active metal oxides, either as single phases or modified structures, were recommended to be applied in such types of scavenging assays of $ABTS^{\bullet+}$ (Figure 6C). The measured $ABTS^{\bullet+}$ scavenging percentages using C.ZnO (36.4 ± 1.45%), M.ZnO (40.7 ± 1.23%), and KNs (21.9 ± 1.78%) are lower than the recognized value using the ascorbic acid as the assessed control (75.4 ± 1.14%) (Figure 6C). However, the obtained ZnO/KNs composite achieved significantly higher scavenging properties (86.8 ± 1.28%) than the ascorbic acid control as well as the individual forms of ZnO and KNs (Figure 6C). This declares the remarkable enhancement effects of the advanced kaolinite nano-scrolls substrate as well as the synthesis method on the activity of the ZnO nanoparticles as common antioxidant agents.

3.2.4. Superoxide Radical Scavenging

Superoxide anion radical ($O_2^{\bullet-}$) is a widely released reactive free oxidizing radical within the cellular organelles such as the mitochondria. The release of the $O_2^{\bullet-}$ radicals is normally associated with their immediate transformation into new species of active species such as hydroxyl radicals ($^{\bullet}OH$) and hydrogen peroxide (H_2O_2). The formation of such $^{\bullet}OH$ radicals at uncontrolled rates and over concentrations within the cells causes severe pathophysiological conditions and numerous species of degenerative diseases and dangerous health risks [55]. Additionally, the secondary reactive products formed during the transformation of $O_2^{\bullet-}$ radical exhibit notable cellular destruction effects on the RNA, DNA, and protein [54]. The biological system of the human body normally provides effective natural defenses against the generated $O_2^{\bullet-}$ radical to maintain safe physiological homeostasis. However, during some diseases, this system cannot provide the required defense function against the $O_2^{\bullet-}$ radical, which makes the effective antioxidant structure critical to overcome the uncontrolled diffusion of the generated $O_2^{\bullet-}$ radical. However, the $O_2^{\bullet-}$ scavenging % using C.ZnO (8.7 ± 1.16%), M.ZnO (11.2 ± 1.13%), and KNs (4.6 ± 0.34%) is lower than the ascorbic acid standard (17.3 ± 1.34%), and the application of the ZnO/KNs composite exhibits significantly higher activity (43.9 ± 1.72%) (Figure 6D). These results are in agreement with the obtained results during the scavenging of the other radicals and recommend strongly the application of the prepared ZnO/KNs as an effective and multi-functional antioxidant agent.

3.3. Antidiabetic Properties

3.3.1. Porcine Pancreatic α-Amylase Inhibition Assay

The potential antidiabetic properties of M.ZnO, KNs, and ZnO/KNs were followed considering their inhibition effects on the commonly evaluated oxidative enzyme including the porcine pancreatic α-amylase enzyme. The α-amylase enzyme is an essential and very active digestive enzyme that exhibits vital effects during the destruction and the breakdown of complex carbohydrate structures such as starch into simple maltose and glucose units [6]. Therefore, the rapid and effective inhibition of the generated α-amylase enzyme is essential to control and reduce the progressive breakdown and destruction of the complex sugar or carbohydrate structures. This in turn will effectively reduce the absorption rate properties of the dietary starch and will regulate the blood sugar as well as postprandial hyperglycemia at acceptable and safe levels [25,55]. The determined inhibition properties are in agreement with the detected behavior during the antioxidation tests (Figure 7A). The determined α-amylase inhibition % using C.ZnO, M.ZnO, and KNs is 40.3 ± 1.66%, 45.6 ± 1.52%, and 27.8 ± 1.86%, respectively (Figure 7A). However, these activities are considerably higher than the obtained results using miglitol (18.3 ± 1.42%), still lower than the determined activity using acarbose (75.2 ± 1.68%) (Figure 7A). The detected inhibition activity of ZnO/KNs (84.3 ± 1.12%) signifies the enhanced properties of the composite as compared to the two assessed drugs (acarbose (75.2 ± 1.68%) and miglitol (18.3 ± 1.42%)) as well as the individual components of the obtained hybrid structure (Figure 7A).

RETRACTED

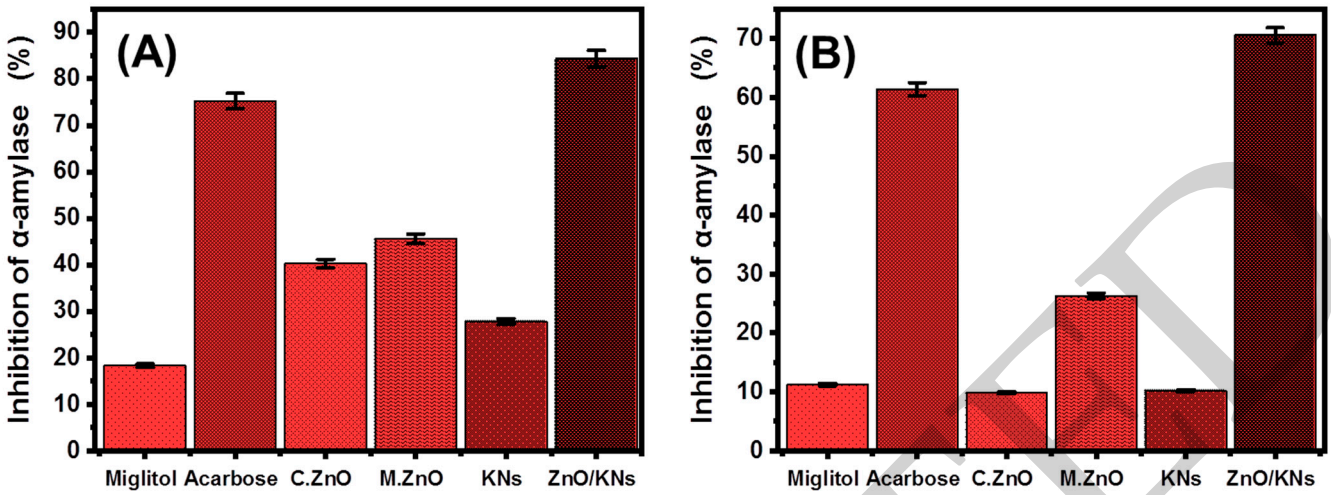


Figure 7. The α-amylase inhibition activities of C.ZnO, M.ZnO, KNs, and ZnO/KNs structures in the presence of acarbose and miglitol as positive controls (the tests were replicated 5 times); (**A**) Porcine pancreatic α-amylase enzyme with significantly higher activity for ZnO/KNs than miglitol; and (**B**) Murine pancreatic α-amylase enzyme with significantly higher activity for ZnO/KNs than miglitol.

The observable enhancement in the actual antidiabetic properties of ZnO/KNs hybrid structure as compared to the separated phases of ZnO can be illustrated based on the reported textural and physicochemical impacts of the used scrolled kaolinite nanoparticles as substrate. The KNs particles induce strongly the surface area, exposure properties, and interactive interfaces of the ZnO nanoparticle in addition to its hindering effect on the agglomeration chances of the supported particle [14,48,56–58]. The aggregation and agglomeration of the commonly tested metal oxides exhibit strong adverse impacts on their documented antidiabetic and biological activities [48]. Based on such inhibition efficiency, the synthetic ZnO/KNs hybrid structure can be recommended as a potentially effective, low-cost, enhanced, safe, and multifunctional antidiabetic agent considering the raw material, fabrication cost, efficiency, and low side effects as compared to the commercially tested drugs [59,60].

3.3.2. Murine Pancreatic α-Amylase Inhibition

The inhibition effects of M.ZnO, KNs, and ZnO/KNs on the murine crude pancreatic α-amylase enzyme were followed to investigate the biological activities of the prepared materials against the metabolically active crude enzyme in addition to previously estimated results against commercial enzymes. By the same method, the inhibition effects were assessed in the synergetic system considering the efficiency of the synthetic ZnO/KNs as well as the integrated individual components (Figure 7B). The application of C.ZnO, M.ZnO, and KNs causes considerable inhibition effects on the crude α-amylase enzyme by 9.8 ± 1.12%, 26.3 ± 1.57%, and 10.2 ± 1.27%, respectively, while the existence of ZnO/KNs induces the inhibition activity to 70.6 ± 1.37%, which is significantly higher than the determined activities using miglitol (11.2 ± 1.61%) as well as acarbose (61.4 ± 1.55%) as commonly used commercial drugs (Figure 7B). Therefore, the synthetic ZnO/KNs structure, as the suggested antidiabetic agent, can be applied effectively against the commercial α-amylase enzyme as well as a metabolically crude enzyme (murine pancreatic).

3.3.3. Pancreatic α-Glucosidase Inhibition

The α-glucosidase enzyme was categorized as one of the most effective and vital enzymes during the metabolic processes of dietary starch and other carbohydrates. Therefore, its inhibition utilizing effective and promising materials was recommended strongly to reduce and regulate the levels of this enzyme. This inhibition effect can control the absorption rates of the simple glucose structures in the blood and cause remarkable sup-

RETRACTED

pression in hyperglycemia [18]. The potential inhibition of α-glucosidase enzyme by M.ZnO, KNs, and ZnO/KNs was studied in comparison with commercial ZnO particles and two of the commonly used drugs (miglitol and acarbose) (Figure 8A). The C.ZnO, M.ZnO, and KNs as inhibition agents have the ability to inhibit the α-glucosidase enzyme by 68.7 ± 1.44%, 74.2 ± 1.37%, and 44.7 ± 1.18%, respectively, while the hybrid ZnO/KNs structure causes a strong enhancement in the achieved inhibition activity to a value of 94.7 ± 1.54% (Figure 8A). The recognized inhibition effect using the ZnO/KNs structure is considerably higher than the recognized effect using miglitol (90.2 ± 1.31%) and close to the determined effect using acarbose (96.4 ± 1.45%) (Figure 8A). This reflects the significant potentiality of the ZnO/KNs structure to be used as an effective antidiabetic agent based on the reported side effects of the commercial drugs as well as their production costs.

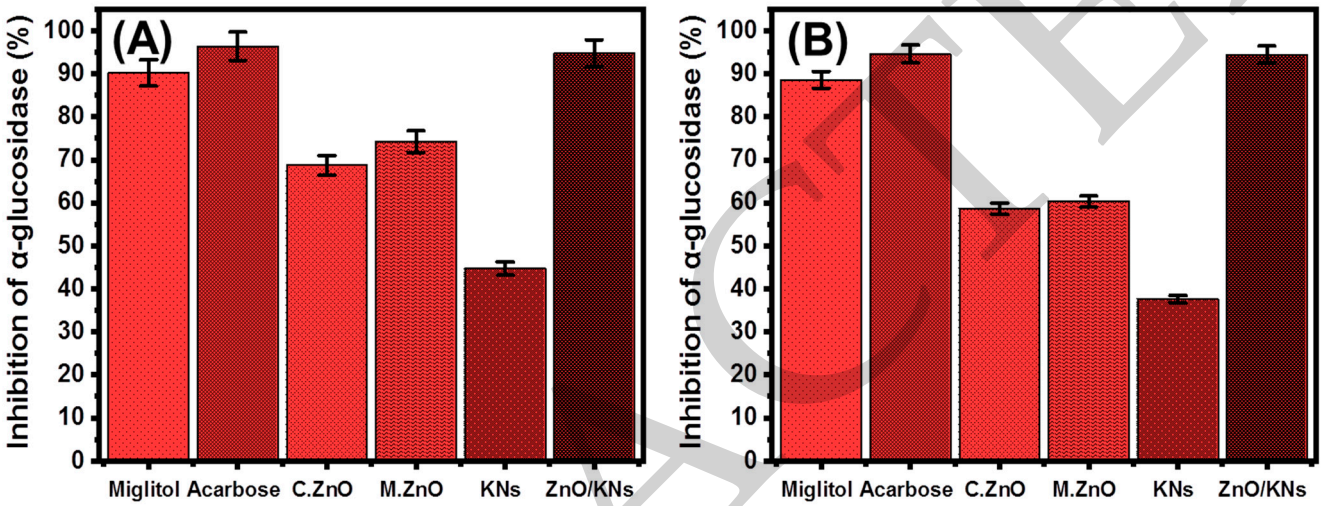


Figure 8. The α-Glucosidase inhibition activities of C.ZnO, M.ZnO, KNs, and ZnO/KNs structures in the presence of acarbose and miglitol as positive controls (the tests were replicated 5 times); (**A**) Pancreatic α-Glucosidase enzyme with considerably higher activity for ZnO/KNs than miglitol; and (**B**) Murine intestinal α-Glucosidase enzyme with considerably higher activity for ZnO/KNs than miglitol.

3.3.4. Murine Intestinal α-Glucosidase Inhibition

The inhibition effects of M.ZnO, KNs, and ZnO/KNs on the intestinal crude α-glucosidase enzyme were inspected to assess the qualification of the products on the crude enzyme as well as the previously tested commercial enzyme. As detected during the investigation of the commercial α-glucosidase enzyme, the inhibition properties of ZnO/KNs are significantly higher than the detected properties of C.ZnO, M.ZnO, and KNs in addition to the commercially tested drugs (Figure 8B). The detected inhibition % using C.ZnO, M.ZnO, and KNs is 58.7 ± 1.46%, 60.3 ± 1.36%, and 37.6 ± 1.32%, respectively (Figure 8B). These results are significantly lower than the recognized inhibition % using the commercially used miglitol (88.6 ± 1.42%) and acarbose (94.6 ± 1.34%) (Figure 8B). However, the determined inhibition % in the existence of ZnO/KNs (95.4 ± 1.64%) reflects its enhancement in the antidiabetic and inhibition activity as compared to the previously evaluated commercial drugs (Figure 8B). Previous studies validated promising antidiabetic properties of ZnO and its significant properties to reduce the levels of glucose compounds in the blood. Moreover, it has remarkable enhancement effects on the glucokinase genes, glucokinase activity, serum insulin, and insulin receptors [61].

3.3.5. Amyloglucosidase Inhibition

The amyloglucosidase enzyme exhibits strong effects during the breakdown and destruction of the complex structure of starch and its absorption rate in the human body.

RETRACTED

Therefore, the significant inhibition of amyloglucosidase enzyme by safe, effective, and low-cost materials will exhibit strong declination properties against the immediate breakdown and transformation of the complex structures of sugar into simple glucose structures with a faster absorption rate [62]. The determined amyloglucosidase inhibition % using C.ZnO, M.ZnO, KNs, and ZnO/KNs is 65.4 ± 1.27%, 69.8 ± 1.62%, 44.7 ± 1.41%, and 95.3 ± 1.32%, respectively (Figure 9). The determined inhibition activity by ZnO/KNs is noticeably higher than the inhibition activity of miglitol (88.3 ± 1.83%) and nearly similar to the recognized inhibition activity of acarbose (95.6 ± 1.72%) (Figure 9). Therefore, the synthetic multifunctional structure of ZnO/KNs that involves supporting ZnO nanoparticles into a substrate of scrolled kaolinite nanoparticles can be recommended as a favorable antidiabetic agent of significant biocompatibility, low health side effects, low fabrication cost, and strong inhibition properties.

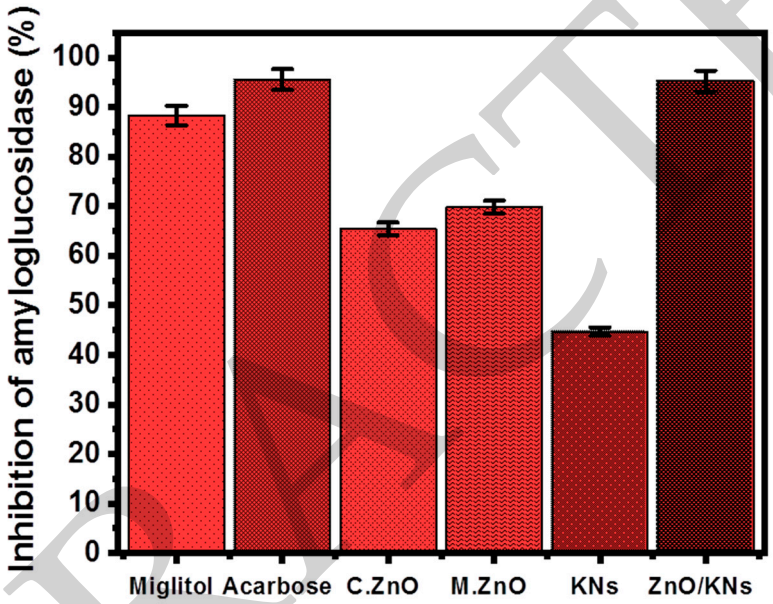


Figure 9. The amyloglucosidase inhibition activities of C.ZnO, M.ZnO, KNs, and ZnO/KNs structures in the presence of acarbose and miglitol as positive controls (the tests were replicated 5 times).

4. Conclusions

ZnO/scrolled kaolinite nanocomposite (ZnO/KNs) was synthesized successfully and characterized as an enhanced antioxidant and antidiabetic agent. The incorporation of KNs as a substrate of ZnO notably enhances the surface area, interactive interface, and charge separation properties of ZnO. These physicochemical enhancement effects in addition to the bioactivity of KNs strongly induces the biological properties of the loaded ZnO. The ZnO/KNs composite displays enhanced scavenging efficiencies towards the common ROS species (DPPH (89.8 ± 1.57%), NO (90.6 ± 1.63%), ABTS (86.8 ± 1.28%), and $O_2^{\bullet -}$ (43.9 ± 1.72%)) and significant inhibition impacts on the oxidative enzymes (porcine α-amylase (84.3 ± 1.92%), crude α-amylase (70.6 ± 1.37%), pancreatic α-glucosidase (94.7 ± 1.54%), crude α-glucosidase (95.4 ± 1.64%), and amyloglucosidase (95.3 ± 1.32%)). It is therefore recommended that the synthetic ZnO/KNs be used as an enhanced antioxidant and antidiabetic agent when considering the cost, efficiencies, and side effects of miglitol and acarbose.

RETRACTED

Supplementary Materials: The following supporting information can be downloaded at: https://www.mdpi.com/article/10.3390/min13040567/s1, Figure S1: EDX mapping of synthetic ZnO/KNs structure; Figure S2: N2 adsorption/desorption isotherm curves of KNs and ZnO/KNs structure.

Author Contributions: Conceptualization, M.R.A., S.B. and H.A.R.; methodology, M.R.A. and H.A.R.; Software, A.A.A. and L.M.A.; validation, M.R.A., S.B., H.A.R., A.A.A. and M.A.; formal analysis, A.A.A., M.A., L.M.A. and M.R.A.; investigation, M.R.A., S.B., H.A.R. and A.A.A.; resources, A.A.A., L.M.A. and M.R.A.; data curation, M.R.A., M.A., L.M.A. and A.A.A.; writing—original draft preparation, M.R.A., M.A., A.A.A., S.B., H.A.R. and L.M.A.; writing—review and editing, M.R.A., H.A.R., A.A.A., S.B. and L.M.A.; visualization, M.R.A., H.A.R. and S.B.; supervision, M.R.A., S.B., A.A.A. and H.A.R.; project administration, M.R.A., H.A.R. and A.A.A.; funding acquisition, S.B. and H.A.R. All authors have read and agreed to the published version of the manuscript.

Funding: This research was funded by Deanship of Scientific Research at Imam Mohammad Ibn Saud Islamic University (IMSIU) grant number [RP-21-09-89].

Data Availability Statement: Data are available upon reasonable, by the Corresponding Authors.

Acknowledgments: The authors extend their appreciation to the Deanship of Scientific Research at Imam Mohammad Ibn Saud Islamic University (IMSIU) for funding and supporting this work through the Research Partnership Program no. (RP-21-09-89).

Conflicts of Interest: The authors declare no conflict of interest.

References

1. Arvanag, F.M.; Bayrami, A.; Habibi-Yangjeh, A.; Pouran, S.R. A comprehensive study on antidiabetic and antibacterial activities of ZnO nanoparticles biosynthesized using *Silybum marianum* L. seed extract. *Mater. Sci. Eng. C* **2019**, *97*, 397–405. [CrossRef] [PubMed]
2. Behl, T.; Kaur, I.; Sehgal, A.; Sharma, E.; Kumar, A.; Grover, M.; Bungau, S. Unfolding Nrf2 in diabetes mellitus. *Mol. Biol. Rep.* **2021**, *48*, 927–939. [CrossRef] [PubMed]
3. Billacura, M.P.; Lavilla, C.J.; Cripps, M.J.; Hanna, K.; Sale, C.; Turner, M.D. β-alanine scavenging of free radicals protects mitochondrial function and enhances both insulin secretion and glucose uptake in cells under metabolic stress. *Adv. Redox Res.* **2022**, *6*, 100050. [CrossRef]
4. Hsu, W.-H.; Chang, H.-M.; Lee, Y.-L.; Prasannan, A.; Hu, C.-C.; Wang, J.-S.; Lai, J.-Y.; Yang, J.M.; Jebaranjitham, N.; Tsai, H.-C. Biodegradable polymer-nanoclay composites as intestinal sleeve implants installed in digestive tract for obesity and type 2 diabetes treatment. *Mater. Sci. Eng. C* **2020**, *110*, 110676. [CrossRef]
5. Sagandira, C.R.; Khasipo, A.Z.; Sagandira, M.B.; Watts, P. An overview of the synthetic routes to essential oral anti-diabetes drugs. *Tetrahedron* **2021**, *96*, 132378. [CrossRef]
6. Robkhob, P.; Ghosh, S.; Bellare, J.; Jamdade, D.; Tang, I.-M.; Thongmee, S. Effect of silver doping on antidiabetic and antioxidant potential of ZnO nanorods. *J. Trace Elem. Med. Biol.* **2020**, *58*, 126448. [CrossRef] [PubMed]
7. Paul, S.; Hajra, D. Study of glucose uptake enhancing potential of fenugreek (*Trigonella foenum* graecum) leaves extract on 3T3 L1 cells line and evaluation of its antioxidant potential. *Pharmacogn. Res.* **2018**, *10*, 347. [CrossRef]
8. Dedvisitsakul, P.; Watla-Iad, K. Antioxidant activity and antidiabetic activities of Northern Thai indigenous edible plant extracts and their phytochemical constituents. *Heliyon* **2022**, *8*, 10740. [CrossRef]
9. Feldman, E.L.; Callaghan, B.C.; Pop-Busui, R.; Zochodne, D.W.; Wright, D.E.; Bennett, D.L.; Bril, V.; Russell, J.W.; Viswanathan, V. Diabetic neuropathy. *Nat. Rev. Dis. Primer* **2019**, *5*, 1–18. [CrossRef]
10. Kim, M.-S.; Jung, Y.S.; Jang, D.; Cho, C.H.; Lee, S.-H.; Han, N.S.; Kim, D.-O. Antioxidant capacity of 12 major soybean isoflavones and their bioavailability under simulated digestion and in human intestinal Caco-2 cells. *Food Chem.* **2022**, *374*, 131493. [CrossRef]
11. Asmat, U.; Abad, K.; Ismail, K. Diabetes mellitus and oxidative stress—A concise review. *Saudi Pharm. J.* **2016**, *24*, 547–553. [CrossRef] [PubMed]
12. Ben Ahmed, Z.; Hefied, F.; Yousfi, M.; Demeyer, K.; Heyden, Y.V. Study of the antioxidant activity of Pistacia atlantica Desf. Gall extracts and evaluation of the responsible compounds. *Biochem. Syst. Ecol.* **2022**, *100*, 104358. [CrossRef]
13. Yilmazer-Musa, M.; Griffith, A.M.; Michels, A.J.; Schneider, E.; Frei, B. Grape Seed and Tea Extracts and Catechin 3-Gallates Are Potent Inhibitors of α-Amylase and α-Glucosidase Activity. *J. Agric. Food Chem.* **2012**, *60*, 8924–8929. [CrossRef] [PubMed]
14. Malik, A.R.; Sharif, S.; Shaheen, F.; Khalid, M.; Iqbal, Y.; Faisal, A.; Aziz, M.H.; Atif, M.; Ahmad, S.; Fakhar-e-Alam, M.; et al. Green synthesis of RGO-ZnO mediated Ocimum basilicum leaves extract nanocomposite for antioxidant, antibacterial, antidiabetic and photocatalytic activity. *J. Saudi Chem. Soc.* **2022**, *26*, 101438. [CrossRef]
15. Singh, T.A.; Sharma, A.; Tejwan, N.; Ghosh, N.; Das, J.; Sil, P.C. A state of the art review on the synthesis, antibacterial, antioxidant, antidiabetic and tissue regeneration activities of zinc oxide nanoparticles. *Adv. Colloid Interface Sci.* **2021**, *295*, 102495. [CrossRef] [PubMed]

RETRACTED

16. Velsankar, K.; Venkatesan, A.; Muthumari, P.; Suganya, S.; Mohandoss, S.; Sudhahar, S. Green inspired synthesis of ZnO nanoparticles and its characterizations with biofilm, antioxidant, anti-inflammatory, and anti-diabetic activities. *J. Mole. Str.* **2022**, *1255*, 132420.
17. Alam, M.W.; Azam, H.; Khalid, N.R.; Naeem, S.; Hussain, M.K.; BaQais, A.; Farhan, M.; Souayeh, B.; Zaidi, N.; Khan, K. Enhanced photocatalytic performance of Ag_3PO_4/Mn-ZnO nanocomposite for the degradation of Tetracycline Hydrochloride. *Crystals* **2022**, *12*, 1156. [CrossRef]
18. Ahmad, M.M.; Mushtaq, S.; Al Qahtani, H.S.; Sedky, A.; Alam, M.W. Investigation of TiO_2 Nanoparticles Synthesized by Sol-Gel Method for Effectual Photodegradation, Oxidation and Reduction Reaction. *Crystals* **2021**, *11*, 1456. [CrossRef]
19. Noohpisheh, Z.; Amiri, H.; Farhadi, S.; Mohammadi-Gholami, A. Green synthesis of Ag-ZnO nanocomposites using Trigonella foenum-graecum leaf extract and their antibacterial, antifungal, antioxidant and photocatalytic properties. *Spectrochim. Acta Part A Mol. Biomol. Spec.* **2020**, *240*, 118595. [CrossRef]
20. Ansari, A.; Ali, A.; Khan, N.; Umar, M.S.; Owais, M. Shamsuzzaman Synthesis of steroidal dihydropyrazole derivatives using green ZnO NPs and evaluation of their anticancer and antioxidant activity. *Steroids* **2022**, *188*, 109113. [CrossRef]
21. Alam, M.W.; Al Qahtani, H.S.; Souayeh, B.; Ahmed, W.; Albalawi, H.; Farhan, M.; Abuzir, A.; Naeem, S. Novel Copper-Zinc-Manganese Ternary Metal Oxide Nanocomposite as Heterogeneous Catalyst for Glucose Sensor and Antibacterial Activity. *Antioxidants* **2022**, *11*, 1064. [CrossRef] [PubMed]
22. Alharthi, F.A.; Alghamdi, A.A.; Al-Zaqri, N.; Alanazi, H.S.; Alsyahi, A.A.; Marghany, A.E.; Ahmad, N. Facile one-pot green synthesis of Ag–ZnO Nanocomposites using potato peeland their Ag concentration dependent photocatalytic properties. *Sci. Rep.* **2020**, *10*, 20229. [CrossRef] [PubMed]
23. Sharma, A.; Nagraik, R.; Sharma, S.; Sharma, G.; Pandey, S.; Azizov, S.; Chauhan, P.K.; Kumar, D. Green synthesis of ZnO nanoparticles using Ficus palmata: Antioxidant, antibacterial and antidiabetic studies. *Results Chem.* **2022**, *4*, 100509. [CrossRef]
24. Saad, A.M.; Abukhadra, M.R.; Ahmed, S.A.-K.; Elzanaty, A.M.; Mady, A.H.; Betiha, M.A.; Shim, J.-J.; Rabie, A.M. Photocatalytic degradation of malachite green dye using chitosan supported ZnO and Ce–ZnO nano-flowers under visible light. *J. Environ. Manag.* **2020**, *258*, 110043. [CrossRef]
25. Yusof, N.A.A.; Zain, N.M.; Pauzi, N. Synthesis of ZnO nanoparticles with chitosan as stabilizing agent and their antibacterial properties against Gram-positive and Gram-negative bacteria. *Int. J. Biol. Macromol.* **2019**, *124*, 1132–1136. [CrossRef]
26. Shaaban, S.; Adam, M.S.S.; El-Metwaly, N.M. Novel organoselenium-based N-mealanilic acid and its zinc (II) chelate: Catalytic, anticancer, antimicrobial, antioxidant, and computational assessments. *J. Mol. Liq.* **2022**, *363*, 119907. [CrossRef]
27. Meer, B.; Andleeb, A.; Iqbal, J.; Ashraf, H.; Meer, K.; Ali, J.S.; Drouet, S.; Anjum, S.; Mehmood, A.; Khan, T.; et al. Bio-Assisted Synthesis and Characterization of Zinc Oxide Nanoparticles from Lepidium Sativum and Their Potent Antioxidant, Antibacterial and Anticancer Activities. *Biomolecules* **2022**, *12*, 855. [CrossRef]
28. Iqbal, T.; Azhar, S.; Zafar, M.; Kiran, H.; Kebaili, I.; Alrobei, H. Synthesis and characterization of Ag-ZnO nano-composites for investigation of variations in the germination of peanut and kidney beans. *Appl. Nanosci.* **2021**, *11*, 2767–2777. [CrossRef]
29. Abukhadra, M.R.; Helmy, A.; Sharaf, M.F.; El-Meligy, M.A.; Soliman, A.T.A. Instantaneous oxidation of levofloxacin as toxic pharmaceutical residuals in water using clay nanotubes decorated by ZnO (ZnO/KNTs) as a novel photocatalyst under visible light source. *J. Environ. Manag.* **2020**, *271*, 111019. [CrossRef]
30. Sabry, R.; AbdulAzeez, O. Hydrothermal growth of ZnO nano rods without catalysts in a single step. *Manuf. Lett.* **2014**, *2*, 69–73. [CrossRef]
31. Singh, R.; Dutta, S. The role of pH and nitrate concentration in the wet chemical growth of nano-rods shaped ZnO photocatalyst. *Nano-Struct. Nano-Objects* **2019**, *18*, 100250. [CrossRef]
32. Chen, Z.; Ma, W.; Lu, G.; Meng, F.; Duan, S.; Zhang, Z.; Wei, L.; Pan, Y. Adsorption of levofloxacin onto mechanochemistry treated zeolite: Modeling and site energy distribution analysis. *Sep. Purif. Technol.* **2019**, *222*, 30–34. [CrossRef]
33. Zhao, Y.; Wang, Y.; Liu, E.; Fan, J.; Hu, X. Bi_2WO_6 nanoflowers: An efficient visible light photocatalytic activity for ceftriaxone sodium degradation. *Appl. Surf. Sci.* **2018**, *436*, 854–864. [CrossRef]
34. Shawky, A.; El-Sheikh, S.M.; Rashed, M.N.; Abdou, S.M.; El-Dosoqy, T.I. Exfoliated kaolinite nanolayers as an alternative photocatalyst with superb activity. *J. Environ. Chem. Eng.* **2019**, *7*, 103174. [CrossRef]
35. Ahn, M.-Y.; Filley, T.R.; Jafvert, C.T.; Nies, L.; Hua, I.; Bezares-Cruz, J. Photodegradation of Decabromodiphenyl Ether Adsorbed onto Clay Minerals, Metal Oxides, and Sediment. *Environ. Sci. Technol.* **2006**, *40*, 215–220. [CrossRef]
36. Kitture, R.; Ghosh, S.; More, P.A.; Date, K.; Gaware, S.; Datar, S.; Chopade, B.A.; Kale, S.N. Curcumin-Loaded, Self-Assembled Aloevera Template for Superior Antioxidant Activity and Trans-Membrane Drug Release. *J. Nanosci. Nanotechnol.* **2015**, *15*, 4039–4045. [CrossRef] [PubMed]
37. Dappula, S.S.; Kandrakonda, Y.R.; Shaik, J.B.; Mothukuru, S.L.; Lebaka, V.R.; Mannarapu, M.; Amooru, G.D. Biosynthesis of zinc oxide nanoparticles using aqueous extract of Andrographis alata: Characterization, optimization and assessment of their antibacterial, antioxidant, antidiabetic and anti-Alzheimer's properties. *J. Mol. Struct.* **2023**, *1273*, 134264. [CrossRef]
38. Sanap, S.P.; Ghosh, S.; Jabgunde, A.M.; Pinjari, R.V.; Gejji, S.P.; Singh, S.; Chopade, B.A.; Dhavale, D.D. Synthesis, computational study and glycosidase inhibitory activity of polyhydroxylated conidine alkaloids—A bicyclic iminosugar. *Org. Biomol. Chem.* **2010**, *8*, 3307–3315. [CrossRef] [PubMed]

RETRACTED

39. Lawande, P.P.; Sontakke, V.A.; Kumbhar, N.M.; Bhagwat, T.R.; Ghosh, S.; Shinde, V.S. Polyhydroxylated azetidine iminosugars: Synthesis, glycosidase inhibitory activity and molecular docking studies. *Bioorganic Med. Chem. Lett.* **2017**, *27*, 5291–5295. [CrossRef] [PubMed]
40. Adly, E.R.; Shaban, M.S.; El-Sherbeeny, A.M.; Al Zoubi, W.; Abukhadra, M.R. Enhanced Congo Red Adsorption and Photo-Fenton Oxidation over an Iron-Impeded Geopolymer from Ferruginous Kaolinite: Steric, Energetic, Oxidation, and Synergetic Studies. *ACS Omega* **2022**, *7*, 31218–31232. [CrossRef]
41. Sayed, M.A.; Ahmed, S.A.; Othman, S.I.; Allam, A.A.; Al Zoubi, W.; Ajarem, J.S.; Abukhadra, M.R.; Bellucci, S. Kinetic, Thermodynamic, and Mechanistic Studies on the Effect of the Preparation Method on the Catalytic Activity of Synthetic Zeolite-A during the Transesterification of Waste Cooking Oil. *Catalysts* **2023**, *13*, 30. [CrossRef]
42. Abukhadra, M.R.; Allah, A.F. Synthesis and characterization of kaolinite nanotubes (KNTs) as a novel carrier for 5-fluorouracil of high encapsulation properties and controlled release. *Inorg. Chem. Commun.* **2019**, *103*, 30–36. [CrossRef]
43. Yang, X.; Wang, J.; El-Sherbeeny, A.M.; AlHammadi, A.A.; Park, W.-H.; Abukhadra, M.R. Insight into the adsorption and oxidation activity of a ZnO/piezoelectric quartz core-shell for enhanced decontamination of ibuprofen: Steric, energetic, and oxidation studies. *Chem. Eng. J.* **2022**, *431*, 134312. [CrossRef]
44. Abukhadra, M.R.; Bakry, B.M.; Adlii, A.; Yakout, S.M.; El-Zaidy, M.E. Facile conversion of kaolinite into clay nanotubes (KNTs) of enhanced adsorption properties for toxic heavy metals (Zn^{2+}, Cd^{2+}, Pb^{2+}, and Cr^{6+}) from water. *J. Hazard. Mater.* **2019**, *374*, 296–308. [CrossRef]
45. Dhall, A.; Self, W. Cerium Oxide Nanoparticles: A Brief Review of Their Synthesis Methods and Biomedical Applications. *Antioxidants* **2018**, *7*, 97. [CrossRef] [PubMed]
46. Sharpe, E.; Andreescu, D.; Andreescu, S. Artificial Nanoparticle Antioxidants. In *Oxidative Stress: Diagnostics, Prevention, and Therapy*; ACS Publications: Washington, DC, USA, 2011; pp. 235–253.
47. Parul, R.; Kundu, S.K.; Saha, P. In vitro nitric oxide scavenging activity of methanol extracts of three Bangladeshi medicinal plants. *Pharma Innov.* **2013**, *1*, 83.
48. Song, Y.; Yang, F.; Ma, M.; Kang, Y.; Hui, A.; Quan, Z.; Wang, A. Green synthesized Se–ZnO/attapulgite nanocomposites using *Aloe vera* leaf extract: Characterization, antibacterial and antioxidant activities. *LWT* **2022**, *165*, 113762. [CrossRef]
49. El-Hack, M.E.A.; El-Saadony, M.T.; Shafi, M.E.; Zabermawi, N.M.; Arif, M.; Batiha, G.E.; Khafaga, A.F.; El-Hakim, Y.M.A.; Al-Sagheer, A.A. Antimicrobial and antioxidant properties of chitosan and its derivatives and their applications: A review. *Int. J. Biol. Macromol.* **2020**, *164*, 2726–2744. [CrossRef]
50. Rabie, A.M.; Abukhadra, M.R.; Rady, A.M.; Ahmed, S.A.; Labena, A.; Mohamed, H.S.H.; Betiha, M.A.; Shim, J.-J. Instantaneous photocatalytic degradation of malachite green dye under visible light using novel green Co–ZnO/algae composites. *Res. Chem. Intermed.* **2020**, *46*, 1955–1973. [CrossRef]
51. Wang, Z.-J.; Xu, J.-J.; Ji, F.-Y.; Luo, S.-Z.; Li, X.-J.; Mu, D.-D.; Jiang, S.-T.; Zheng, Z. Fabrication and characterization of soy β-conglycinin-dextran-polyphenol nanocomplexes: Improvement on the antioxidant activity and sustained-release property of curcumin. *Food Chem.* **2022**, *395*, 133562. [CrossRef]
52. Adersh, A.R.; Kulkarni, S.; Ghosh, P.; More, B.A.; Chopade, M.; Gandhi, N. Surface defect rich ZnO quantum dots as antioxidant inhibitingα-amylase and α-glucosidase: A potential anti-diabetic nanomedicine. *J. Mater. Chem. B* **2015**, *3*, 4597–4606.
53. Abukhadra, M.R.; AlHammadi, A.A.; Khim, J.S.; Ajarem, J.S.; Allam, A.A. Enhanced decontamination of Levofloxacin residuals from water using recycled glass based a green zinc oxide/mesoporous silica nanocomposite; adsorption and advanced oxidation studies. *J. Clean. Prod.* **2022**, *356*, 131836. [CrossRef]
54. Liu, Y.; Ying, D.; Cai, Y.; Le, X. Improved antioxidant activity and physicochemical properties of curcumin by adding ovalbumin and its structural characterization. *Food Hydrocoll.* **2017**, *72*, 304–311. [CrossRef]
55. Hamasaki, T.; Kashiwagi, T.; Imada, T.; Nakamichi, N.; Aramaki, S.; Toh, K.; Morisawa, S.; Shimakoshi, H.; Hisaeda, Y.; Shirahata, S. Kinetic Analysis of Superoxide Anion Radical-Scavenging and Hydroxyl Radical-Scavenging Activities of Platinum Nanoparticles. *Langmuir* **2008**, *24*, 7354–7364. [CrossRef]
56. Xie, J.; Wang, N.; Dong, X.; Wang, C.; Du, Z.; Mei, L.; Yong, Y.; Huang, C.; Li, Y.; Gu, Z.; et al. Graphdiyne Nanoparticles with High Free Radical Scavenging Activity for Radiation Protection. *ACS Appl. Mater. Interfaces* **2018**, *11*, 2579–2590. [CrossRef] [PubMed]
57. Shu, G.; Xu, D.; Xie, S.; Chang, L.-J.; Liu, X.; Yang, J.; Li, Y.; Wang, X. The antioxidant, antibacterial, and infected wound healing effects of ZnO quantum dots-chitosan biocomposite. *Appl. Surf. Sci.* **2023**, *611*, 155727. [CrossRef]
58. Deng, J.; Wang, J.; Hu, H.; Hong, J.; Yang, L.; Zhou, H.; Xu, D. Application of mesoporous calcium silicate nanoparticles as a potential SD carrier to improve the solubility of curcumin. *J. Dispers. Sci. Techno.* **2022**, 1–9. [CrossRef]
59. Vinotha, V.; Iswarya, A.; Thaya, R.; Govindarajan, M.; Alharbi, N.S.; Kadaikunnan, S.; Khaled, J.M.; Al-Anbr, M.N.; Vaseeharan, B. Synthesis of ZnO nanoparticles using insulin-rich leaf extract: Anti-diabetic, antibiofilm and anti-oxidant properties. *J. Photochem. Photobio. B Biol.* **2019**, *197*, 111541. [CrossRef]
60. Rehana, D.; Mahendiran, D.; Kumar, R.S.; Rahiman, A.K. In Vitro antioxidant and antidiabetic activities of zinc oxide nanoparticles synthesized using different plant extracts. *Bioprocess Biosyst. Eng.* **2017**, *40*, 943–957. [CrossRef]

RETRACTED

61. Alkaladi, A.; Abdelazim, A.M.; Afifi, M. Antidiabetic activity of zinc oxide and silver nanoparticles on streptozotocin-induced diabetic rats. *Int. J. Mol. Sci.* **2014**, *15*, 2015–2023. [CrossRef]
62. Dhobale, S.; Thite, T.; Laware, S.L.; Rode, C.V.; Koppikar, S.J.; Ghanekar, R.-K.; Kale, S.N. Zinc oxide nanoparticles as novel alpha-amylase inhibitors. *J. Appl. Phys.* **2008**, *104*, 094907. [CrossRef]

Disclaimer/Publisher's Note: The statements, opinions and data contained in all publications are solely those of the individual author(s) and contributor(s) and not of MDPI and/or the editor(s). MDPI and/or the editor(s) disclaim responsibility for any injury to people or property resulting from any ideas, methods, instructions or products referred to in the content.

RETRACTED